Preparation and Characterization of Magnetic Material/Chitosan Composite Modified with Glycidyl-Trimethylammonium Chloride

Feri Mukhayani[1], Eko Sri Kunarti[1], Yuichi Kamiya[2], and Nuryono Nuryono[1*]

[1]*Department of Chemistry, Faculty of Mathematics and Natural Sciences, Universitas Gadjah Mada, Sekip Utara, Yogyakarta 55281, Indonesia*

[2]*Research Faculty of Environmental Earth Science, Hokkaido University, Nishi 5, Kita 10, Kita-ku, Sapporo 060-0810, Japan*

* ***Corresponding author:***

email: nuryono_mipa@ugm.ac.id

Received: September 6, 2023
Accepted: December 21, 2023

DOI: 10.22146/ijc.88758

Abstract: *Glycidyl-trimethylammonium chloride (GTMAC) containing quaternary ammonium (QA) groups is commonly used as a base catalyst for any organic reaction. This research prepared a novel composite of GTMAC attached to chitosan-coated magnetic material (MM/Chi/GTMAC) using a precipitation method. The effect of chitosan and GTMAC contents on MM/chi/GTMAC properties was studied, where the chitosan content varied from 0, 0.3, 0.5, 1.0, and 3.0 mol, and GTMAC varied from 0, 0.3, 0.8, 1.0, 1.5, and 3 mL with the constant mass of MM (0.4640 g). The physicochemical and morphological properties were characterized with FTIR, SEM-EDX, XRD, TGA, UV-vis, AAS, and zeta-sizer, and the magnetic strength was simply tested with an external magnet. The result showed that a mixture containing chitosan and GTMAC of 0.358 g and 1.5 mL was an optimum composition, in which MM/chi(0.5)/GTMAC(1.5) has high thermal stability, low chitosan and Fe solubility, and optimum content of QA (0.284 mol/g) without loss of magnetic strength. The higher the amount of chitosan, the lower the magnetic properties, and the higher the GTMAC did not increase the QA content. Therefore, the composite produced has the potential to be a novel heterogeneous base catalyst that is quickly recovered from any organic reaction media.*

Keywords: *glycidyl-trimethylammonium chloride; MM modified chitosan; physicochemical properties*

■ INTRODUCTION

The use of quaternary ammonium salt (QASs) in various advanced applications has been approved due to its excellent properties. QASs contain positively charged nitrogen atoms (N^+), which can be synthesized from the N^+ on the straight chain or in the aromatic ring that covalently binds four carbon atoms. The unique structure of QASs provides them with physicochemical effects, especially solubilization [1] and dispersion [2] effects. QASs have been extensively utilized in the sectors of water treatment [3], agriculture [4], phase-transfer catalyst [5], and medical (as antibacterial agents) [6]. Glycidyl-trimethylammonium chloride (GTMAC) is a family of QASs that can be used in many technological and chemical uses because of its unique properties. Because of the presence of the $-^+N(CH_3)_3$ group, GTMAC has a considerable affinity to water [7]. GTMAC also has an epoxide ring useful for further modification [8]. GTMAC is commonly applied as a base catalyst because it contains a chloride anion that acts as a Lewis base [9-10]. As a homogenous catalyst, it must be immobilized with polymers to separate GTMAC easily from the reaction media.

GTMAC can link with other materials through chemical reactions and ring opening of the epoxide group [11-12]. Previous studies have investigated the covalent bonding of GTMAC to polymeric materials. In this decade, GTMAC has been used to modify various polymeric materials. Cellulose is reacted with GTMAC [13], chitosan is connected with GTMAC [14], *p*-aramid fibers are attached to GTMAC [15], and poly(ethylene glycol)-diacrylate (PEGDA), trimethylolpropane-tri-

acrylate (TMPTA), and trimethylolpropane tris(3-mercaptopropionate) (TMPTMP) crosslinked with GTMAC [16]. Among these polymeric materials, chitosan is the most promising and abundant material due to its biodegradability, biocompatibility, and non-toxicity [17]. The cationic character of chitosan on its surface can be shown in neutral conditions. Chitosan can be applied in several areas, especially adsorption and catalysis, because it is biocompatible with a wide pH range [18]. In the modification, chitosan, comprising many reactive amine and hydroxyl groups, successfully reacted with the epoxy group of GTMAC [19]. Generally, composite chitosan/GTMAC with desirable permeability often fails to meet selective criteria and properties. In addition, the performances of most polymeric water composites like chitosan are a strong function of the water concentration. High water concentration causes swelling [20-21], but low water concentration makes the benchmark dehydration chitosan composite material glassy [22]. Thus, proper and simple design experiments are challenging to obtain the chitosan/GTMAC composite with high stability.

Adding magnetic material (MM) to a composite can simplify separating it from a system using an external magnet [23-24]. Natural MM isolated from iron sands provides strong magnetic properties due to highly magnetic minerals [25]. Nevertheless, due to low stability in an acidic aqueous solution, it is necessary to modify MM to produce a more stable magnetic composite material [26]. The stabilization of MM can be increased by chitosan coating [27], but using an inappropriate amount of chitosan can reduce the magnetic properties of MM [28]. Adding chitosan to MM, which is not proportional, produced an irregular structural morphology [29]. Then, the particle size tends to be large, and the particle aggregation is difficult to control [30]. The properties and structure of composites can influence their performance [31]. The poor physicochemical properties, low chemical-thermal stability, and high swelling of MM-modified chitosan/GTMAC in an aqueous system must be prevented. Therefore, this research studies the modification of chitosan-coated MM with GTMAC to produce MM/Chi/GTMAC through the precipitation method. The influence of chitosan and GTMAC contents on the properties of the composite was evaluated, and the optimum composition resulting in the composite with high thermal and acidic stability, optimum QASs content, and without magnetic strength loss was obtained.

■ EXPERIMENTAL SECTION

Materials

The magnetic material was isolated from iron sand collected in Meliwis Beach, Kebumen, Central Java, Indonesia, using a procedure as previously reported [32]. Chitosan (*N*-deacetylation degree 75%), sodium hydroxide (NaOH, > 98%), and acetic acid (CH_3COOH, glacial 100%) were obtained from Merck, Germany. GTMAC was procured from Sigma Aldrich. All chemical agents and materials were used as received. In short, CH_3COOH 1% v/v is used to dissolve chitosan powder.

Instrumentation

Infrared spectra of the modified chitosan were recorded with attenuated total reflectance-Fourier-transform infrared (ATR-FTIR) spectrometer (Nicolet iS5, USA) with 16 scans at a 4 cm^{-1} of resolution over a scanning range of 4000–400 cm^{-1}. Elemental composition and morphology of the materials were determined using scanning electron microscope-energy dispersive X-ray (SEM-EDX) (JSM-6510LA-EX-3618OD3A, JEOL, USA) with an accelerating voltage of 5 kV. X-ray fluorescence spectroscopy (XRF) performed on a spectrometer (SPECTRO Analytical Instruments GmbH, Germany) equipped with a 50 W Pd X-ray tube was used to determine the chemical composition of iron sand and the modified samples. X-ray diffraction was performed using an X-ray diffractometer (Bruker D8 Advance diffractometer, Bruker AXS, Germany). XRD diffraction patterns were obtained using Cu-Kα radiation under 40 kV and 25 mA. Thermogravimetric analysis (TGA) of all samples was performed using a Pyris 1 TGA thermal analyzer (Perkin Elmer, USA). The samples were heated at 25–500 °C at 20 °C min^{-1} under a flowing nitrogen atmosphere at a purge rate of

20 mL min^{-1}. The total Fe content in the modified sample was determined after 50 mg of the sample was dissolved in 10 mL of various pH solutions by the atomic absorption spectrometer (Analytical Jena). Solubilized chitosan in various pHs was characterized by UV-vis spectroscopy in a wavelength range of 200–600 nm. The size and surface charge of the particles were analyzed by dynamic light scattering (DLS, Zeta-sizer Nano ZS90, Malvern Instruments Ltd., UK) equipped with a He-Ne laser beam at 293 nm. The refractive index (RI) and the detection angle were set at 1.540 and 173° backscatter, respectively. The magnetic property of the samples was measured simply by using an external magnet (dimension 20 mm × 4 mm × 2 mm) with magnetics strength categories: strong if it can be attracted with a magnet in less than 15 s; moderate if it can be tempted with an external magnet within 15–45 s; and weak if it can be attracted with an external magnet for more than 45 s (composite mass was constant = 1 g).

Procedure

Preparation of MM from iron sands

The MM was prepared from iron sands using a procedure previously reported with minor modification [32]. MM sample was separated from the iron sand (25 g) with an external magnet attraction and pounded in a mortar with a pestle. The resulting powder (~10 g) was sieved using a sieve with 200 mesh in screen size and washed using distilled water until the filtrate was colorless. Next, the powder sand was dried at 95 °C for 10 h. The material was heated in 50 mL HCl 1 M solution at 60 °C for 5 h, and then the mixture was added to NaOH 1 M solution until pH 10. The precipitate was washed with distilled water until neutral and then dried at 90 °C for 10 h to obtain MM. After drying, the sample was collected in vials for further characterization and modification.

Manufacture of MM/Chi/GTMAC composite

First of all, the chitosan solution was made by mixing 0.3580 g of chitosan powder in 50 mL of 1% CH_3COOH solution (w/v in H_2O) using a magnetic stirrer with a speed of 400 rpm until it became homogenous. Second, 0.4640 g of MM in 3 mL HCl 1 M solution was added to the previously prepared chitosan solution, and the mixture was dispersed using ultrasonic assistance at room temperature (25 °C) for 60 min. Then, the mixture was stirred (400 rpm) at a temperature of 60 °C for 4 h. After that, the solution was added with 1.5 mL GTMAC. Next, the mixture was stirred (400 rpm) at room temperature for 1 h. The precipitate was separated and dried at 60 °C for 18 h. After drying, the sample was collected in a vial for further characterization. The procedure was repeated with the various concentrations of chitosan and GTMAC, as shown in Table 1. The reaction routes of the composite preparation are illustrated in Fig. 1.

■ RESULTS AND DISCUSSION

Characteristics of MM

Chemical composition

The iron sand was characterized by XRF to recognize the mineral contained in the iron sand from Meliwis Beach, Kebumen, Central Java.

Table 1. The composition data of the composites with various concentrations of (a) chitosan and (b) GTMAC

[a] Material code	[a] Mass of		[b] Material	[b] GTMAC	[b] Composite
	chitosan (g)	composite (g)		volume (mL)	mass (g)
MM/chi(0.0)/GTMAC(1.5)	0.0000	1.9446	MM/chi(0.5)/GTMAC(0.0)	0.00	0.8028
MM/chi(0.1)/GTMAC(1.5)	0.0895	2.0335	MM/chi(0.5)/GTMAC(0.3)	0.25	1.0538
MM/chi(0.3)/GTMAC(1.5)	0.1790	2.1401	MM/chi(0.5)/GTMAC(0.8)	0.75	1.5520
MM/chi(0.5)/GTMAC(1.5)	0.3580	2.3128	MM/chi(0.5)/GTMAC(1.5)	1.50	2.3090
MM/chi(1.0)/GTMAC(1.5)	0.7160	2.6524	MM/chi(0.5)/GTMAC(2.0)	2.00	2.7920
MM/chi(3.0)/GTMAC(1.5)	2.1588	4.1028	MM/chi(0.5)/GTMAC(3.0)	3.00	3.8057

[a] Mass of MM = 0.4640 g (constant); volume of GTMAC = 1.50 mL (constant)

[b] Mass of MM = 0.4640 g (constant); mass of chitosan = 0.3580 g (constant)

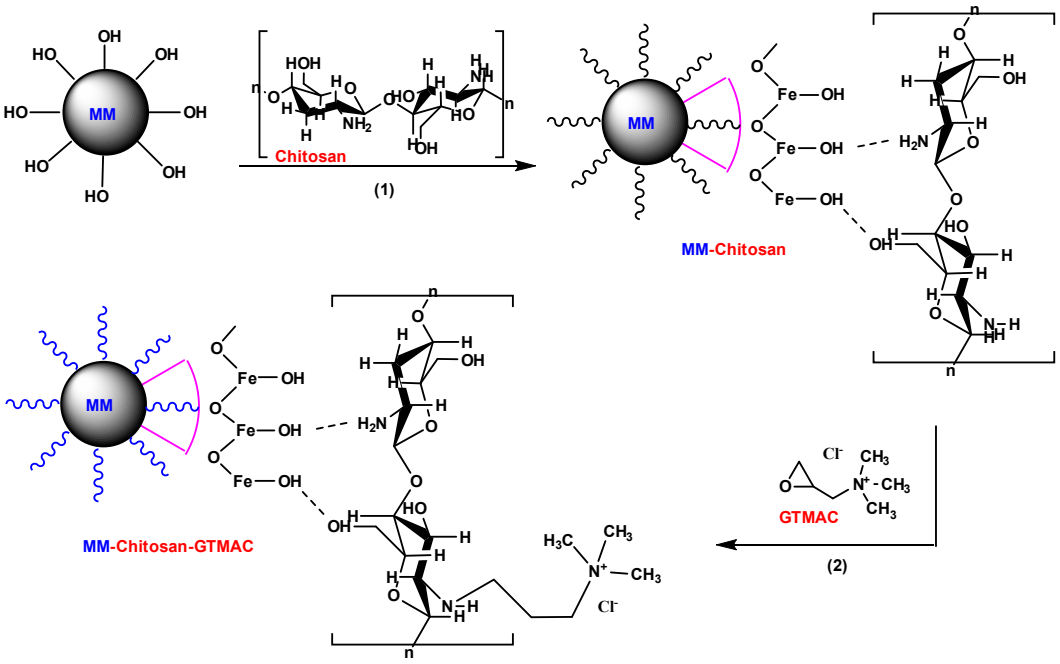

Fig 1. Reaction scheme for the preparation of MM/chi/GTMAC composite

Apart from the element iron (Fe), there were other elements, namely silicon (Si), calcium (Ca), titanium (Ti), chloride (Cl), and phosphorus (P). Based on the results shown in Fig. 2**,** Fe was the most dominant element in the iron sand. Ti was also found in the iron sand with low concentration. The elemental composition of Fe increased from 70.72 to 88.76% after the extracting process. In addition, the content of other minerals such as Si, Ca, Cl, and P was not significantly present. This outcome indicates that the magnetic material extraction has been carried out successfully because the impurities have been reduced [33]. The Fe content in this iron sand was close to 80 %, which follows previous studies [34-35], so it is possible to use it as a modifying MM.

XRD and FTIR spectra of MM

The MM diffraction pattern is shown in Fig. 3(a). The XRD peak data corresponded to magnetite from the powder diffraction file (PDF) from JCPDS No. 01-075-044 [36]. The 2θ peaks of 30.0, 35.4, 43.0, 53.4, 56.9, and 62.5° corresponded to the lattice planes of [2 2 0], [3 1 1],

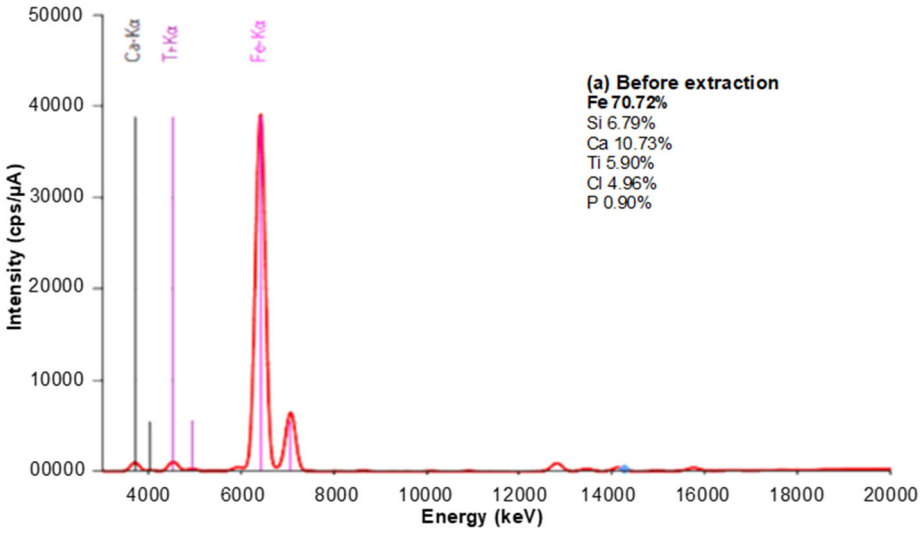

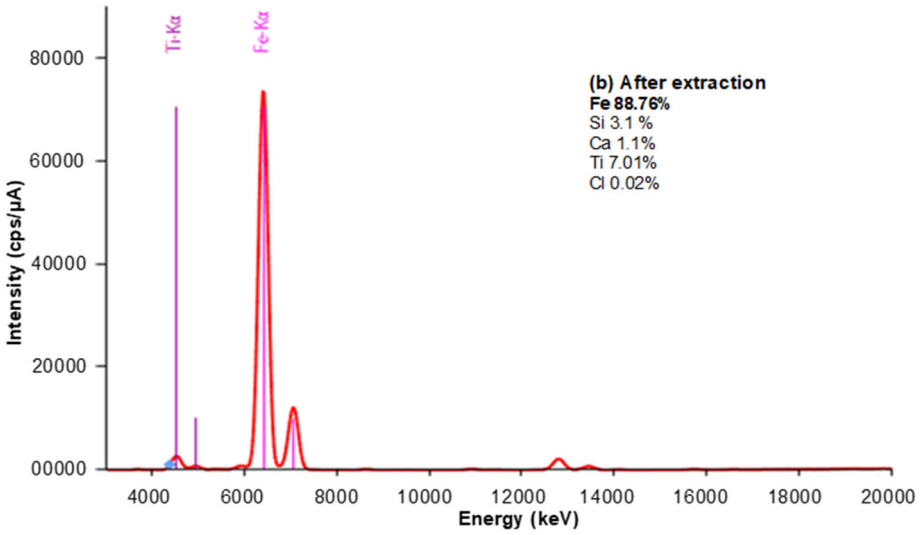

Fig 2. Elemental composition of iron sand (a) before and (b) after extraction

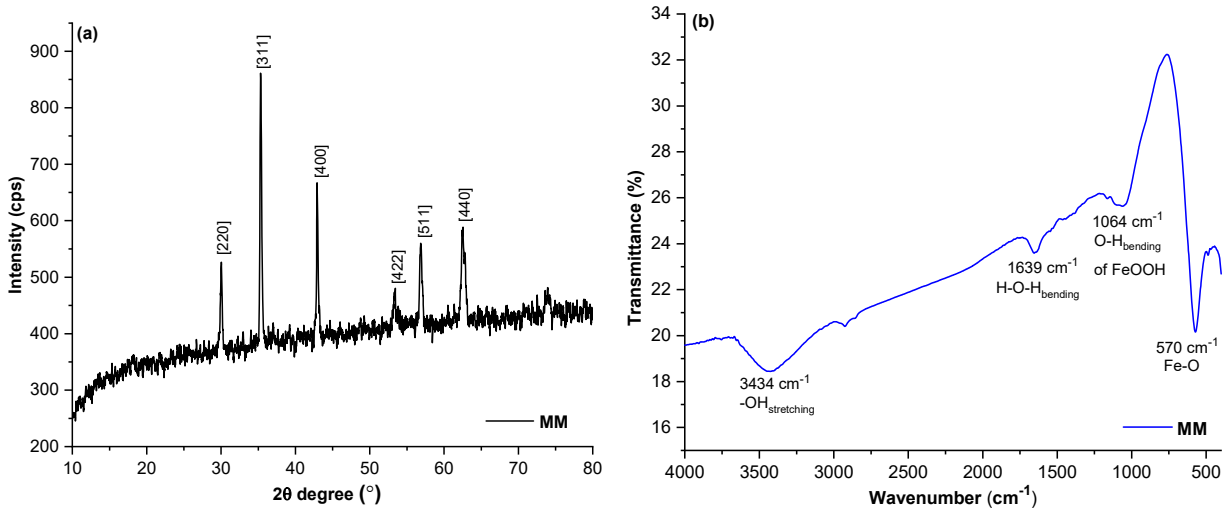

Fig 3. (a) XRD pattern and (b) IR spectrum of MM

[4 0 0], [4 2 2], [5 1 1], and [4 4 0], respectively. In addition, there was a peak with low intensity, around 74°, which was the XRD peak of Ti [37]. Based on the literature, this sample contained a small amount of Ti with a type of titanomagnetite mineral [38]. Next, the IR spectrum of the MM is shown in Fig. 3(b). The wavenumber of 570 cm^{-1} was a stretching vibration of Fe–O from magnetite, characterizing an absorption band around the wavenumber of 600 cm^{-1} [39]. Another specific peak of magnetite can also be identified from the bending vibration of H–O–H at a wavenumber of 1,639 cm^{-1}. A broad band at a wavenumber of 3,434 cm^{-1} relates to the –OH stretching vibration of Fe–OH. An absorption peak at the wavenumber of 1,056 cm^{-1} correlated to –OH asymmetric bending in FeOOH [40].

Effect of Chitosan and GTMAC Contents on MM/Chi/GTMAC Properties

Based on Table 2, it is shown that the magnetic strength decreased when the composite powder was agglomerated as chitosan concentration increased. As a result, there was an increase in chitosan viscosity. In solution, the chitosan polymer is a cationic polyelectrolyte due to the protonation of the amine in an acidic medium [41]. As a result, the higher the density of chitosan crosslinking, the greater the expansion of the polymer

Table 2. The magnetic property of MM/chi/GTMAC with various concentrations of chitosan

Material	Composite form	Magnetic strength
MM/chi(0.0)/GTMAC(1.5)	powder	Strong
MM/chi(0.1)/GTMAC(1.5)	powder	Strong
MM/chi(0.3)/GTMAC(1.5)	powder	Strong
MM/chi(0.5)/GTMAC(1.5)	powder	Strong
MM/chi(1.0)/GTMAC(1.5)	aggregate	Moderate
MM/chi(3.0)/GTMAC(1.5)	aggregate	Weak

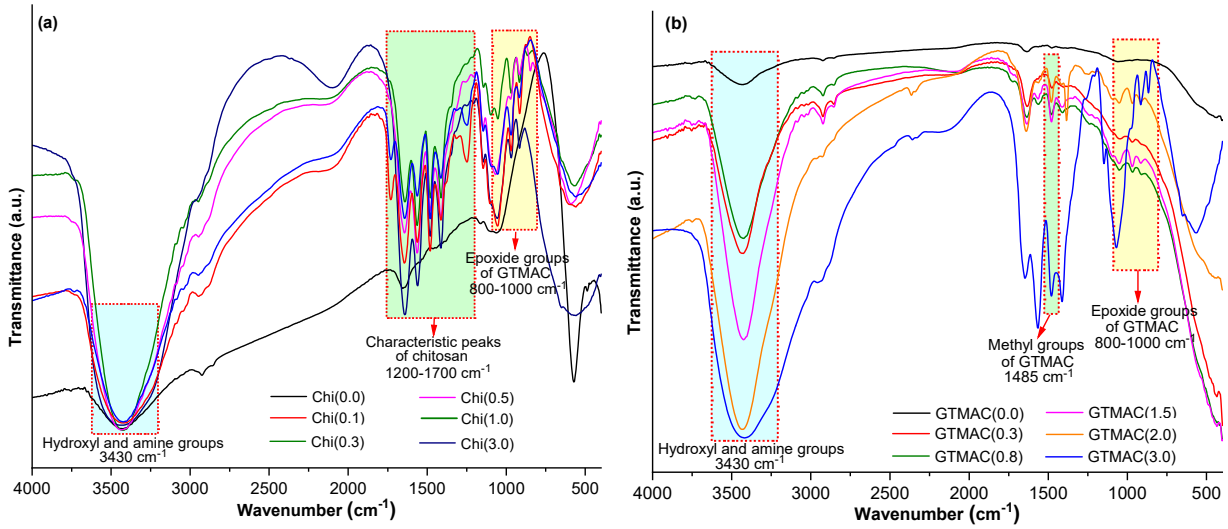

Fig 4. FTIR spectra of MM/chi/GTMAC with various amount of (a) chitosan and (b) GTMAC

chains, thus leading to structural density [42-44]. The amount of chitosan must be optimum in designing MM/chitosan composites. If the amount of chitosan is minimal, then the MM is not adequately coated. If the amount of chitosan is too much, the magnetic properties of MM become weaker. The composite started to agglomerate when the concentration of chitosan was 1 mol. We conclude that the optimum chitosan concentration was 0.5 because this composite has good dispersion (powder form) and high magnetic strength. This conclusion followed previous research that polymer composites have large aggregation clusters because the reactivity of the magnetic materials is greater. Therefore, the amount of polymer used must be considered for its impact on the magnetic strength of the materials [45]. The GTMAC variation composite's magnetic strength was not measured because adding GTMAC with various contents in this study did not change the MM magnetic strength significantly.

Functional groups

IR spectra of composites with various chitosan contents are shown in Fig. 4(a). It can be observed that the characteristics of chitosan and GTMAC appeared at the wavenumber of 800–1800 cm^{-1}. There were absorption peaks of functional groups of chitosan [46], including –C–O–C (1,001 cm^{-1}), –CO (1,159 cm^{-1}), –CH_2– (1,416 cm^{-1}, 1,336 cm^{-1}), –CO (1,647 cm^{-1}), –C–H (2,900 cm^{-1}), and –NH_2, –OH (3,400 cm^{-1}). The absorption peaks of functional groups of GTMAC [11] include C–O–C epoxides (861, 928, and 961 cm^{-1}), C–H from CH_3 (1,475 cm^{-1}), and N–H (3,356 cm^{-1}). Fe–O was observed at the wavenumber of 680 cm^{-1} [47]. All composites have the three characters of MM, chitosan, and GTMAC, except for the MM/chi(0)/GTMAC. There was a small GTMAC peak and a very sharp Fe–O peak in MM/chi(0)/GTMAC. This indicates that the role of chitosan as a linker agent between MM and GTMAC is essential [31]. Based on FTIR analysis, it was impossible

to determine the most optimum composite because each material has absorption peak characteristics that did not differ significantly.

Fig. 4(b) shows the FTIR spectra of the MM/chi(0.5)/GTMAC composite with various concentrations of GTMAC. The peaks around 1,410 and 1,570 cm^{-1} are the absorption peaks of amino I and amino II functional groups of chitosan, respectively [14]. The intensity of these peaks increased when GTMAC was added. It confirms that the GTMAC interacted with chitosan by reacting the epoxy group of GTMAC with the amine group of chitosan [2-3]. From the FTIR spectra in Fig. 4(b), new absorption peaks appeared in the wavenumber of 900–1,200 cm^{-1} in the MM/chi(0.5)/GTMAC(1.5) composite. These peaks are related to characteristic peaks of epoxide and methyl groups of GTMAC [48]. The intensity of the absorption peak increased gradually with the increase of GTMAC concentration in the composite [18,49-50].

Crystallinity

Variations of chitosan contents added affected the crystallinity of MM. Chitosan is an amorphous material with diffraction peaks at 2θ 10.62° and 19.86° [51]. Based on Fig. 5(a), the contents of chitosan affected the MM crystallinity. The greater the chitosan concentration added, the lower the MM crystallinity appeared [52]. The amorphous character of chitosan increased as the chitosan concentration increased. From Fig. 5(a), the most optimum material was MM/chi(0.5)/GTMAC(1.5). This selection was based on the high intensity of MM peaks, which could still be observed, and the amorphous nature of chitosan did not dominate.

The composite diffraction pattern of MM/chi(0.5)/GTMAC with various GTMAC concentrations is shown in Fig. 5(b). The 2θ peaks of MM appeared in all composites. Overall, there was no change in intensity or shift of the 2θ peaks from the MM diffraction peaks, but there was a slight shifting of the peaks. This indicates that GTMAC did not significantly affect MM crystallinity because the GTMAC attached to chitosan [48].

Morphology

SEM images of the MM/Chi/GTMAC with the various chitosan contents were observed in Fig. 6. The SEM image of the GTMAC variation composite was not measured because adding GTMAC with various contents in this study did not change the surface morphology of chitosan-coated MM. The SEM images show differences in the surface structure of composites with various chitosan contents. Without chitosan, it can be observed that MM/chi(0)/GTMAC(1.5) has a cubic structure of MM coating by a sprinkling of GTMAC. The MM particles appeared to be connected to each other after the presence of chitosan. Furthermore, the surface structure became denser and tighter as the chitosan increased.

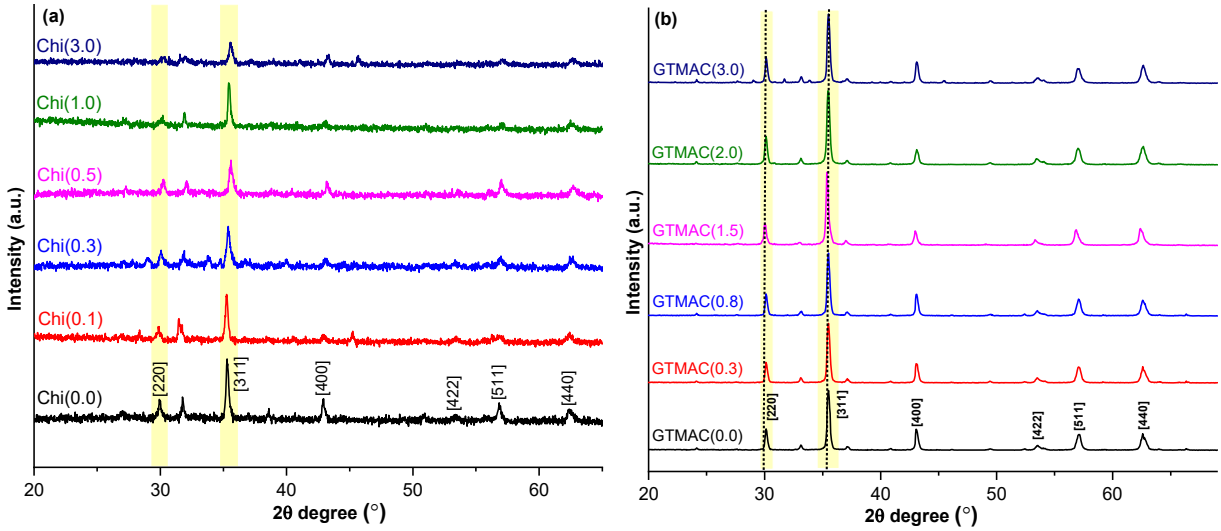

Fig 5. XRD spectra of MM/chi/GTMAC with various contents of (a) chitosan and (b) GTMAC

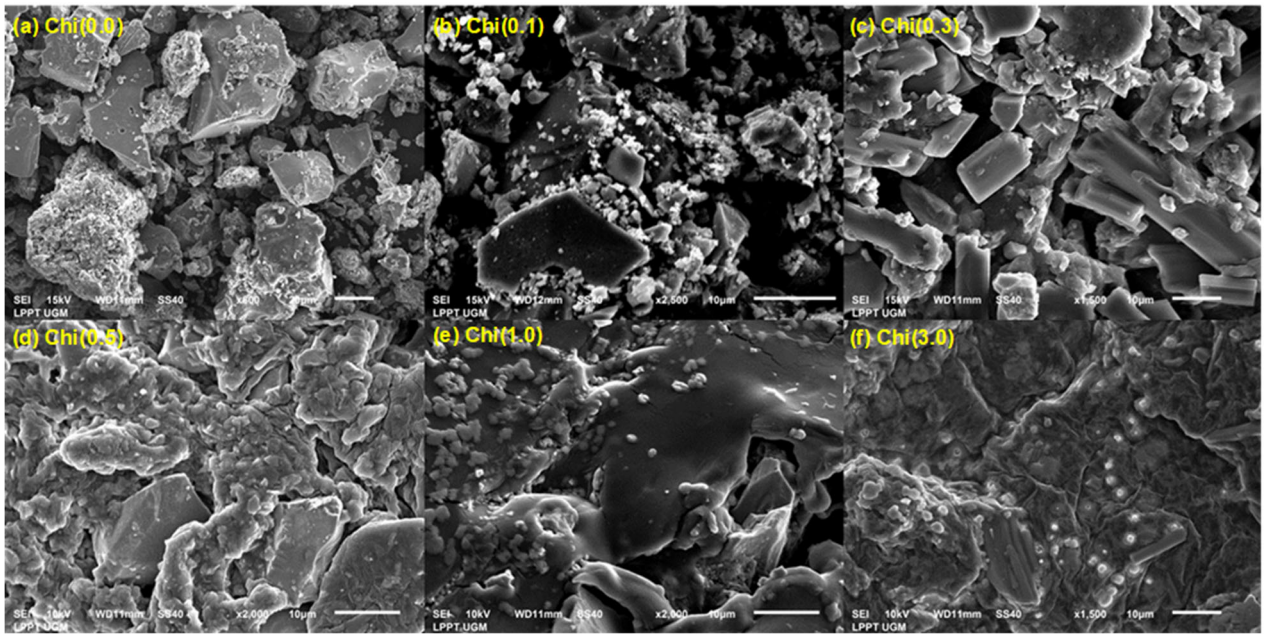

Fig 6. SEM images of MM/chi(x)/GTMAC(1.5) with various chitosan contents

The MM particle in the MM/Chi(0.1)/GTMAC was covered by a thicker and broader layer of 0.1 mol of chitosan and 1.5 mL of GTMAC. MM/Chi(0.3)/GTMAC has an elongated cubic structure linked by GTMAC and chitosan with a concentration of 0.3 mol. Chitosan in MM/chi(0.5)/GTMAC(1.5), MM/chi(1.0)/GTMAC(1.5), and MM/chi(3.0)/GTMAC(1.5) composites coated the MM material producing a layer structure as the result of material agglomeration. The presence of MM in MM/chi(0.5)/GTMAC(1.5) could be observed, but the presence of MM could not be observed in the MM/chi(1.0)/GTMAC(1.5) and MM/chi(3.0)/GTMAC (1.5) composites because the surface was entirely covered by chitosan. It is appropriate with the magnetic strength data of the composite, which is shown in Table 2.

Elemental analysis

Based on the composition data from EDX analysis in Table 3, it can be seen that the concentration of Fe atom in the MM/chi/GTMAC(1.5) composites with various chitosan contents decreased due to the increase of chitosan content. Conversely, there was an increase in C and N atoms of chitosan. This correlated with the SEM analysis, where a chitosan layer covered the MM particles. Furthermore, the highest composition of the Cl atom indicates that the amount of GTMAC was successfully bound to chitosan. It can be concluded to be the optimum composition of the MM/chi/GTMAC(1.5) composite based on SEM-EDX analysis.

The elemental composition of MM/chi(0.5)/GTMAC composites with various GTMAC

Table 3. The atomic composition of MM/chi(x)/GTMAC from EDX analysis

Sample	Atomic composition (%)							
	Fe	Ti	Ca	Si	C	N	O	Cl
MM/chi(0.0)/GTMAC	35.67	2.10	2.18	4.21	10.23	4.89	40.16	0.56
MM/chi(0.1)/GTMAC	26.86	3.20	2.22	3.50	18.12	9.12	35.10	1.98
MM/chi(0.3)/GTMAC	23.43	1.98	1.97	2.75	25.56	10.03	32.14	2.14
MM/chi(0.5)/GTMAC	10.20	2.50	1.69	2.15	27.04	11.20	29.28	2.29
MM/chi(1.0)/GTMAC	13.92	1.89	1.09	2.10	30.09	14.67	34.12	2.12
MM/chi(3.0)/GTMAC	6.07	3.89	1.14	1.17	35.30	17.67	33.10	1.66

contents was analyzed using an XRF instrument, and the results are presented in Table 4. It identifies that the Fe composition of MM decreased, and the Cl composition increased by adding chitosan and GTMAC because chitosan and GTMAC modified the MM. The increase of GTMAC at the concentrations of 1.5 to 2.0 and 3.0 mL did not significantly increase the number of Cl atoms. This indicates that the excess of GTMAC did not bind with chitosan. Thus, the optimum GTMAC concentration was 1.5 mL.

Thermal stability

TGA analysis was performed to estimate the amount of chitosan bound to the MM surface, and the TGA curves of MM/chi/GTMAC(1.5) composites with variations in chitosan content are shown in Fig. 7(a). The TGA curve of MM/chi/GTMAC has two steps of mass reduction of H_2O evaporation and chitosan-GTMAC decomposition at temperatures below 100 °C and 170–230 °C, respectively [53-54]. From the mass reduction percentage of MM/chi(0)/GTMAC(1.5), it can be observed that the composite without chitosan was unstable because the decomposition of GTMAC was very high. The composite with the best stability can be seen from the most negligible degradation of the composite [55]. MM/chi(0.5)/GTMAC (1.5) showed the slightest degradation, around 45.76%.

The TGA curves of the MM/chi(0.5)/GTMAC composites with various contents of GTMAC are shown in Fig. 7(b). There were two mass reduction steps for all composites. The mass loss in the first step occurs at a temperature below 100 °C, while the mass loss in the second step occurs at a temperature of 170–300 °C. The first step correlated with the physically adsorbed water molecules on the composite. The second step corresponded with the degradation of chitosan and GTMAC molecules. The MM/chi(0.5)/GTMAC(1.5) composite showed the slightest mass degradation. This indicates that the composite was more stable due to the strong bond between chitosan and GTMAC.

Table 4. The element composition of MM/chi(0.5)/GTMAC(y) from XRF analysis

Sample	Mass of element composition (%)		
	Fe	Ti	Cl
MM/chi(0.5)/GTMAC(0.0)	91.62	6.24	2.14
MM/chi(0.5)/GTMAC(0.3)	86.54	6.74	6.72
MM/chi(0.5)/GTMAC(0.8)	76.23	5.97	17.80
MM/chi(0.5)/GTMAC(1.5)	71.48	5.23	23.29
MM/chi(0.5)/GTMAC(2.0)	70.93	4.92	24.15
MM/chi(0.5)/GTMAC(3.0)	65.90	5.43	28.67

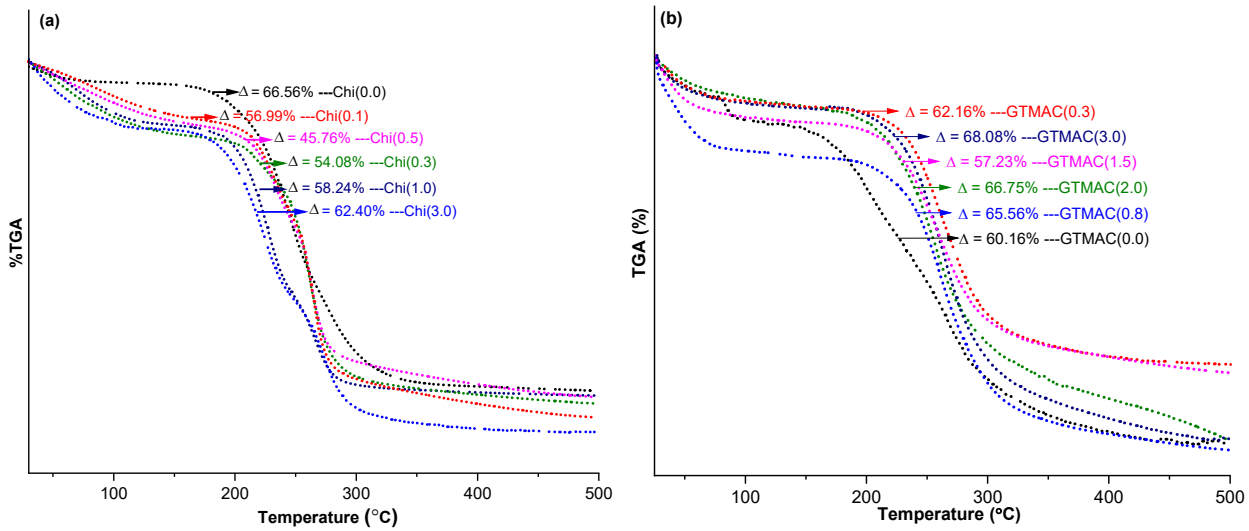

Fig 7. TGA curves of MM/chi/GTMAC with various contents of (a) chitosan and (b) GTMAC

Particle size and zeta potential

The particle size and zeta potential of the MM/chi/GTMAC(1.5) with various chitosan concentrations are shown in Fig. 8(a). The particle size increased with the increase in chitosan concentration. The increased chitosan concentration increased the thickness of the chitosan covering on the MM [56]. Next, the zeta potential value indicates that the greater the chitosan concentration, the more positive the surface charge of the composite. Since chitosan is responsive to pH, the composite's outer layer, mainly chitosan, can change its surface charge [57]. This shows that the increase in the concentration of chitosan, the more chitosan was functionalized on the MM surface.

PSA and zeta potential of various MM/chi(0.5)/GTMAC composites with various contents of GTMAC are presented in Fig. 8(b). The results show that the particle size of the composites did not significantly differ with the increase in GTMAC concentration. Still, there was a slight increase due to increasing GTMAC concentration. The rise of GTMAC increased the thickness of MM coating. Increasing GTMAC concentration caused effective binding of amine groups of chitosan with the epoxide groups of GTMAC. MM/chitosan without GTMAC modification or MM/chi(0.5)/GTMAC(0) initially has a zeta potential of 34.07 mV. After adding GTMAC with a concentration from 0.3 to 3.0 mL, the zeta potential increased due to the increase of the positive ammonium group of GTMAC. The optimum composition was obtained from the smallest size particle as a stable composite from PSA and zeta potential analysis.

Acidic stability

Chitosan solubility. A study of the chitosan release in the solution with a pH range of 1–7 was carried out using a UV-vis spectrometer. Fig. 9(a) shows the composites' UV-vis spectra. MM/chi(0)/GTMAC(1.5) has no absorbance peak at 200–300 nm wavelength because the composite did not contain chitosan. In other composites that contained chitosan, there was a change in the intensity of the absorbance peaks when the pH solution was changed. All composites that contained chitosan were stable at pH 1–4 because of the consistency of the absorbance value. Interestingly, the amount of dissolved chitosan in MM/chi(1.5)/GTMAC(1.5) and MM/chi(3.0)/GTMAC (1.5) decreased significantly as the pH of the solution increased to be a stable composite. Chitosan is not protonated at the high pH [58]. The stability of the composite was evaluated from the percentage of chitosan, which did not release when it was dissolved [59]. The percentage of chitosan that is undissolved is shown in Fig. 9(b), indicating MM/chi(0.5)/GTMAC(1.5) was the most stable composite in pH 2–7. Meanwhile, the undissolved chitosan in other composites increased with changes in pH.

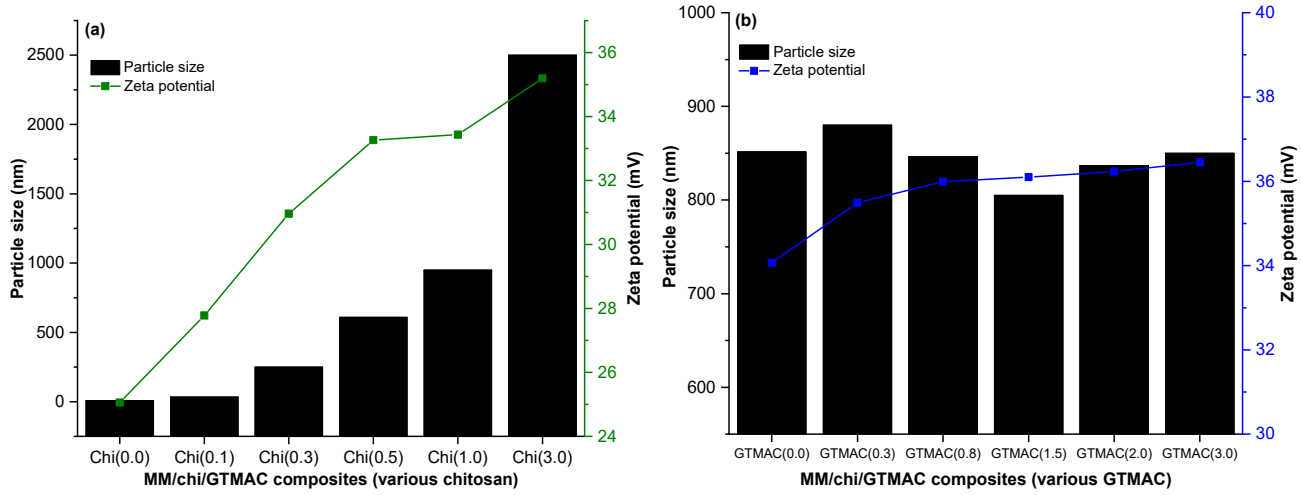

Fig 8. Particle size and zeta potential of MM/chi/GTMAC with various concentrations of (a) chitosan and (b) GTMAC

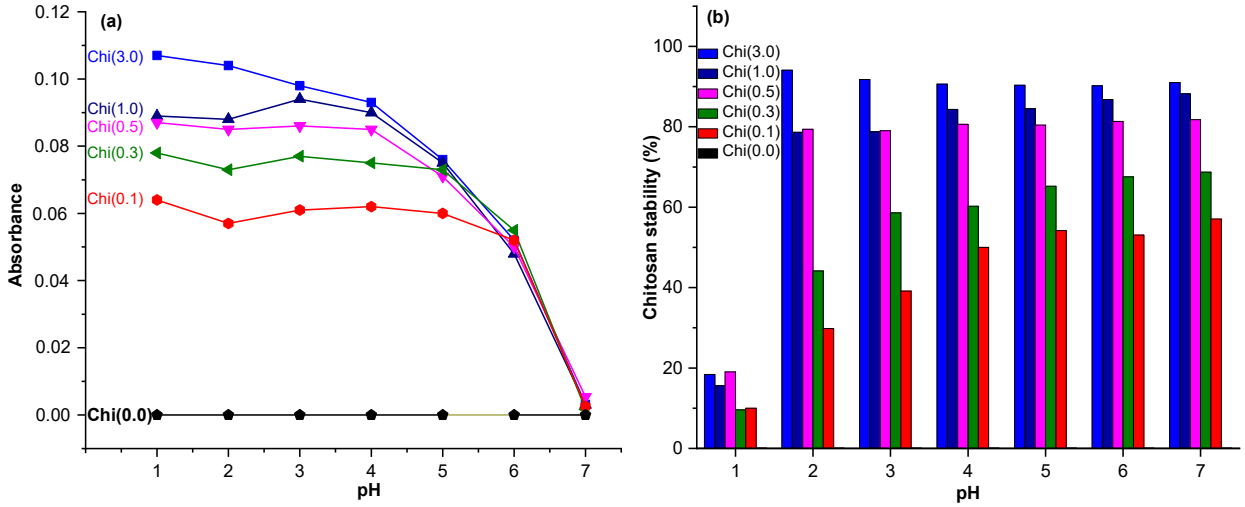

Fig 9. (a) Chitosan absorbance and (b) undissolved chitosan of MM/chi(x)/GTMAC(1.5) composites with various contents of chitosan

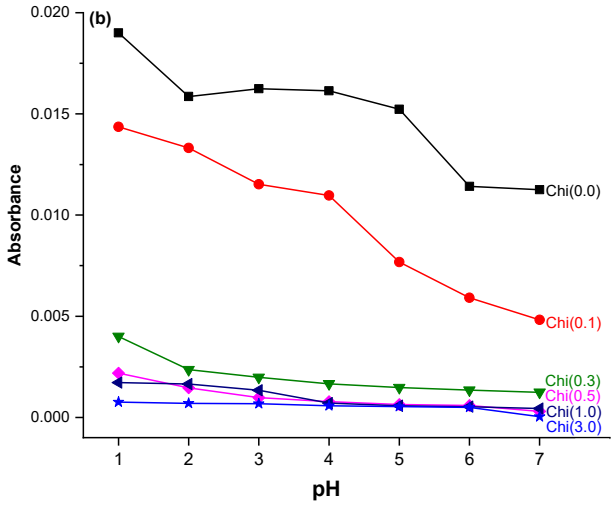

Fig 10. Absorbance data of Fe released of MM/chi(x)/GTMAC(1.5)

Iron (Fe) solubility. The stability of the composite was also evaluated based on the amount of Fe released from MM in various pHs of the solutions. According to the magnetite stability test by Tokarčíková et al. [60], magnetite was unstable at pH 2–4. The less stable property of MM becomes a weakness when MM is applied in an acidic solution system. In this research, the MM stability was improved by chitosan coating. The absorbance of Fe released from MM/chi/GTMAC(1.5) with different chitosan content is shown in Fig. 10. Overall, the released Fe decreased when the chitosan content was increased. The composite is stable if the absorbance of released Fe is constant in various pH [61]. Hence, the composites with a chitosan content higher than 0.5 are observed to be stable.

By referring to the thorough experimental data presented and discussed, it can be summarized that the recommended composition to produce the composite with high physicochemical properties (low solubility of chitosan and Fe, and thermal stability of composite), uniformity of the structure, and optimum content of quaternary ammonium groups without loss of magnetic strength was 0.5 g of chitosan, 1.5 mL of GTMAC and 0.464 g of MM.

■ CONCLUSION

A composite of MM/Chi/GTMAC has been successfully synthesized with a robust technique (precipitation) between GTMAC and MM using chitosan as the linker agent. The optimum composition resulting in the composite with high thermal stability, low chitosan and Fe solubility, optimum quaternary ammonium groups (0.284 mol/g), and without loss of magnetic property was 0.464 g, 0.358 g, and 1.5 mL of MM, chitosan, and GTMAC, respectively. Therefore, this composite is being tested as a catalyst for esterification reaction and has potential as an adequate heterogeneous base.

■ ACKNOWLEDGMENTS

All authors thank The Ministry of Education, Culture, Research, and Technology of Indonesia for funding the research through the PMDSU project (contract no. 2192/UN1/DITLIT/Dit-Lit/PT.01.03/2023).

■ CONFLICT OF INTEREST

The authors have no conflict of interest.

■ AUTHOR CONTRIBUTIONS

Nuryono conceived the presented idea, discussed this work's findings, and revised the manuscript. Yuichi Kamiya and Eko Sri Kunarti supervised and discussed the findings of this work. Feri Mukhayani designed, conducted, and wrote the original manuscript. All authors agreed to the final version of this manuscript.

■ REFERENCES

[1] Matsuoka, K., Takahashi, N., Yada, S., and Yoshimura, T., 2019, Solubilization ability of star-shaped trimeric quaternary ammonium bromide surfactant, *J. Mol. Liq.*, 291, 111254.

[2] Jiang, H., Xiang, G., Khoso, S.A., Xie, J., Huang, K., and Xu, L., 2019, Comparative studies of quaternary ammonium salts on the aggregation and dispersion behavior of kaolinite and quartz, *Minerals*, 9 (8), 473.

[3] Hora, P.I., Pati, S.G., McNamara, P.J., and Arnold, W.A., 2020, Increased use of quaternary ammonium compounds during the SARS-CoV-2 pandemic and beyond: Consideration of environmental implications, *Environ. Sci. Technol. Lett.*, 7 (9), 622–631.

[4] Zhang, X., Kong, H., Zhang, X., Jia, H., Ma, X., Miao, H., Mu, Y., and Zhang, G., 2021, Design and production of environmentally degradable quaternary ammonium salts, *Green Chem.*, 23 (17), 6548–6554.

[5] Qian, D., and Sun, J., 2019, Recent progress in asymmetric ion-pairing catalysis with ammonium salts, *Chem. - Eur. J.*, 25 (15), 3740–3751.

[6] Almeida e Silva, T., Gorup, L.F., de Araújo, R.P., Fonseca, G.G., Martelli, S.M., de Oliveira, K.M.P., Faraoni, L.H., de Arruda, E.G.R., Gomes, R.A.B., da Silva, C.H.M., and de Arruda, E.J., 2020, Synergy of biodegradable polymer coatings with quaternary ammonium salts mediating barrier function against bacterial contamination and dehydration of eggs, *Food Bioprocess Technol.*, 13 (12), 2065–2081.

[7] Sajjan, A.M., Jeevan Kumar, B.K., Kittur, A.A., and Kariduraganavar, M.Y., 2013, Development of novel grafted hybrid PVA membranes using glycidyltrimethylammonium chloride for pervaporation separation of water–isopropanol mixtures, *J. Ind. Eng. Chem.*, 19 (2), 427–437.

[8] Puangkaew, T., Booranabunyat, N., Kiatkamjornwong, S., Thanyasrisuung, P., and Hoven, V.P., 2022, Amphiphilic quaternized chitosan: Synthesis, characterization, and anti-cariogenic biofilm property, *Carbohydr. Polym.*, 277, 118882.

[9] Li, C., Zhao, S., Yao, X., He, L., Xu, S., Shen, X., and Yao, Z., 2022, The catalytic mechanism of intercalated chlorine anions as active basic sites in MgAl-layered double hydroxide for carbonyl sulfide hydrolysis, *Environ. Sci. Pollut. Res.*, 29 (7), 10605–10616.

[10] Cheng, F., Yang, J., Yan, L., Zhao, J., Zhao, H., Song, H., and Chou, L., 2018, Impact of chloride ions on the oxidative coupling of methane over Li/SnO_2 catalyst, *React. Kinet., Mech. Catal.*, 125 (2), 675–688.

[11] Sekhavat Pour, Z., Makvandi, P., and Ghaemy, M., 2015, Performance properties and antibacterial activity of crosslinked films of quaternary ammonium modified starch and poly(vinyl alcohol), *Int. J. Biol. Macromol.*, 80, 596–604.

[12] Istiningrum, R.B., Santosa, S.J., and Nuryono, N., 2021, preparation of magnetic/silica/quarternary-chitosan by sol-gel method and its stability in various pH Medium, *Rasayan J. Chem.*, 14 (4), 2767–2775.

[13] Kang, C.K., Kim, S.S., Kim, S., Lee, J., Lee, J.H., Roh, C., and Lee, J., 2016, Antibacterial cotton fibers treated with silver nanoparticles and quaternary ammonium salts, *Carbohydr. Polym.*, 151, 1012–1018.

[14] Sajjan, A.M., Premakshi, H.G., and Kariduraganavar, M.Y., 2015, Synthesis and characterization of

GTMAC grafted chitosan membranes for the dehydration of low water content isopropanol by pervaporation, *J. Ind. Eng. Chem.*, 25, 151–161.

[15] Kang, C., Ahn, D., Roh, C., Kim, S.S., and Lee, J., 2017, Development of synergistic antimicrobial coating of *p*-aramid fibers using Ag nanoparticles and glycidyltrimethylammonium chloride (GTAC) without the aid of a crosslinking agent, *Polymers*, 9 (8), 357.

[16] Beyler-Çiğil, A., Birtane, H., Şen, F., and Kahraman, M.V., 2021, Transparent and flexible antibacterial photocrosslinked thin films against the *S. aureus* and *E. coli* pathogen bacteria, *Mater. Today Commun.*, 27, 102463.

[17] Taher, M.A., Omer, A.M., Hamed, A.M., Ali, A.M., Tamer, T.M., and Mohy Eldin, M.S., 2019, Development of smart alginate/chitosan grafted microcapsules for colon site-specific drug delivery, *Egypt. J. Chem.*, 62 (6), 1037–1045.

[18] Dragan, E.S., and Dinu, M.V., 2019, Advances in porous chitosan-based composite hydrogels: Synthesis and applications, *React. Funct. Polym.*, 146, 104372.

[19] Jiang, Z., Yu, Y., and Wu, H., 2006, Preparation of CS/GPTMS hybrid molecularly imprinted membrane for efficient chiral resolution of phenylalanine isomers, *J. Membr. Sci.*, 280 (1-2), 876–882.

[20] Boudouaia, N., Bendaoudi, A.A., Mahmoudi, H., Saffaj, T., and Bengharez, Z., 2022, Swelling and adsorption properties of crosslinked chitosan-based filmkinetic, thermodynamic and optimization studies, *Desalin. Water Treat.*, 255, 56–67.

[21] Nawaz, A., Ullah, S., Alnuwaiser, M.A., Rehman, F.U., Selim, S., Al Jaouni, S.K., and Farid, A., 2022, Formulation and evaluation of chitosan-gelatin thermosensitive hydrogels containing 5FU-alginate nanoparticles for skin delivery, *Gels*, 8 (9), 537.

[22] Lewandowska, K., and Szulc, M., 2022, Rheological and film-forming properties of chitosan composites, *Int. J. Mol. Sci.*, 23 (15), 8763.

[23] Martha, A.A., Sutarno, S., and Nuryono, N., 2022, One-pot synthesis and characterization of gold nanoparticle-embedded natural magnetic particles/chitosan composite, *Solid State Phenom.*, 339, 11–17.

[24] Martha, A.A., Permatasari, D.I., Dewi, E.R., Wijaya, N.A., Kunarti, E.S., Rusdiarso, B., and Nuryono, N., 2022, Natural magnetic particles/chitosan impregnated with silver nanoparticles for antibacterial agents, *Indones. J. Chem.*, 22 (3), 620–629.

[25] Karbeka, M., Koly, F.V.L., and Tellu, N.M., 2021, Characterization of magnetic content from Puntaru Beach iron sand, *AIP Conf. Proc.*, 2349 (1), 020026.

[26] Fiejdasz, S., Gilarska, A., Horak, W., Radziszewska, A., Strączek, T., Szuwarzyński, M., Nowakowska, M., and Kapusta, C., 2021, Structurally stable hybrid magnetic materials based on natural polymers – preparation and characterization, *J. Mater. Res. Technol.*, 15, 3149–3160.

[27] Lu, Q., Choi, K., Nam, J.D., and Choi, H.J., 2021, Magnetic polymer composite particles: Design and magnetorheology, *Polymers*, 13 (4), 512.

[28] Smit, M., and Lutz, M., 2020, Polymer-coated magnetic nanoparticles for the efficient capture of *Mycobacterium tuberculosis* (Mtb), *SN Appl. Sci.*, 2 (10), 1658.

[29] Tao, H.C., Li, S., Zhang, L.J., Chen, Y.Z., and Deng, L.P., 2019, Magnetic chitosan/sodium alginate gel bead as a novel composite adsorbent for Cu(II) removal from aqueous solution, *Environ. Geochem. Health*, 41 (1), 297–308.

[30] Zhang, L., Gao, C., Wang, Z., Xie, F., Chen, Y., Meng, L., and Tang, X., 2023, Structure and properties of thermomechanically processed chitosan-based biomimetic composite materials: Effect of chitosan molecular weight, *ACS Sustainable Chem. Eng.*, 11 (2), 708–717.

[31] Chapa González, C., Navarro Arriaga, J.U., and García Casillas, P.E., 2021, Physicochemical properties of chitosan-magnetite nanocomposite obtained with different pH, *Polym. Polym. Compos.*, 29 (Suppl. 9), 1009–1016.

[32] Nuryono, N., Miswanda, D., Sakti, S.C.W., Rusdiarso, B., Krisbiantoro, P.A., Utami, N.,

Otomo, R., and Kamiya, Y., 2020, Chitosan-functionalized natural magnetic particle@silica modified with (3-chloropropyl)trimethoxysilane as a highly stable magnetic adsorbent for gold(III) ion, *Mater. Chem. Phys.*, 255, 123507.

[33] Kono, M.C., Batu, M.S., Kedang, Y.I., and Seran, R., 2021, XRF and XRD Investigation for the results of the extraction of mud volcano from napan village into silica, *JKPK*, 6 (3), 317.

[34] Ramadhan, M., Fahmiati, F., Alrum, A., and La Ode Muhammad Zuhdi, M., 2023, Free solvent isolation of Fe_3O_4 from magnetic material iron sand utilizing high-energy ball milling as adsorben remazol turquoise blue G-133 and remazol red RB-133, *Acta Chim. Asiana*, 6 (1), 269–278.

[35] Prasetyowati, R., Ariswan, A., Warsono, W., and Dewi, N., 2019, Synthesis and characterization of magnetite nanoparticles (Fe_3O_4) based on iron sand from Glagah Kulon Progo Yogyakarta via coprecipitation method with variations in the dissolution duration, *The Science and Science Education International Seminar Proceedings 2019*, Yogyakarta State University, Yogyakarta, Indonesia, 27-28 September 2019, 1–7.

[36] Denison, M.I.J., Raman, S., Duraisamy, N., Thangavelu, R.M., Riyaz, S.U.M., Gunasekaran, D., and Krishnan, K., 2015, Preparation, characterization and application of antibody-conjugated magnetic nanoparticles in the purification of begomovirus, *RSC Adv.*, 5 (121), 99820–99831.

[37] Park, K.B., Choi, J., Na, T.W., Kang, J.W., Park, K., and Park, H.K., 2019, Oxygen reduction behavior of HDH TiH_2 powder during dehydrogenation reaction, *Metals*, 9 (11), 1154.

[38] Kirana, K.H., Ghazali, M., Septiana, L.A.E.S., Fitriani, D., Agustine, E., Fajar, S.J., and Nugraha, M.G., 2020, Karakterisasi mineral magnetik sedimen sungai citarum hilir melalui analisa sifat magnetik, mineralogi serta morfologi magnetik, *Positron*, 10 (2), 131–139.

[39] Prasdiantika, R., and Susanto, S., 2017, Preparasi dan penentuan jenis oksida besi pada material magnetik pasir besi Lansilowo, *Jurnal Teknosains*, 6 (1), 7–15.

[40] Amini, M., Mousazade, Y., Zand, Z., Bagherzadeh, M., and Najafpour, M.M., 2021, Ultra-small and highly dispersive iron oxide hydroxide as an efficient catalyst for oxidation reactions: A Swiss-army-knife catalyst, *Sci. Rep.*, 11 (1), 6642.

[41] Dhanavel, S., Mathew, S.A., and Stephen, A., 2019, "Grafted Chitosan Systems for Biomedical Applications" in *Functional Chitosan: Drug Delivery and Biomedical Applications*, Eds. Jana, S., and Jana, S., Springer Singapore, Singapore, 385–413.

[42] Wang, Q.Z., Chen, X.G., Liu, N., Wang, S.X., Liu, C.S., Meng, X.H., and Liu, C.G., 2006, Protonation constants of chitosan with different molecular weight and degree of deacetylation, *Carbohydr. Polym.*, 65 (2), 194–201.

[43] Aranaz, I., Alcántara, A.R., Civera, M.C., Arias, C., Elorza, B., Heras Caballero, A., and Acosta, N., 2021, Chitosan: An overview of its properties and applications., *Polymers*, 13 (19), 3256.

[44] Melro, E., Antunes, F.E., da Silva, G.J., Cruz, I., Ramos, P.E., Carvalho, F., and Alves, L., 2021, Chitosan films in food applications. Tuning film properties by changing acidic dissolution conditions, *Polymers*, 13 (1), 1.

[45] Aslibeiki, B., Eskandarzadeh, N., Jalili, H., Ghotbi Varzaneh, A., Kameli, P., Orue, I., Chernenko, V., Hajalilou, A., Ferreira, L.P., and Cruz, M.M., 2022, Magnetic hyperthermia properties of $CoFe_2O_4$ nanoparticles: Effect of polymer coating and interparticle interactions, *Ceram. Int.*, 48 (19, Part A), 27995–28005.

[46] Adewuyi, S., Bisiriyu, I.O., Akinremi, C.A., and Amolegbe, S.A., 2017, Synthesis, spectroscopic, surface and catalytic reactivity of chitosan supported Co(II) and its zerovalentcobalt nanobiocomposite, *J. Inorg. Organomet. Polym. Mater.*, 27 (1), 114–121.

[47] Suyanta, S., Sutarno, S., Nuryono, N., Rusdiarso, B., Kunarti, E.S., Kusumastuti, H., and Kurnia, L., 2019, Superparamagnetic nanocomposite of magnetite-chitosan using oleic acid as anti-agglomeration and glutaraldehyde as crosslinkage agent, *Indones. J. Chem.*, 19 (1), 133–142.

[48] Borandeh, S., Laurén, I., Teotia, A., Niskanen, J., and Seppälä, J., 2023, Dual functional quaternary chitosans with thermoresponsive behavior: Structure-activity relationships in antibacterial activity and biocompatibility, *J. Mater. Chem. B*, 11 (47), 11300–11309.

[49] Cho, J., Grant, J., Piquette-Miller, M., and Allen, C., 2006, Synthesis and physicochemical and dynamic mechanical properties of a water-soluble chitosan derivative as a biomaterial, *Biomacromolecules*, 7 (10), 2845–2855.

[50] Wang, B.M., Liu, Y., Ren, P., Xia, B., Ruan, K.B., Yi, J.B., Ding, J., Li, X.G., and Wang, L., 2011, Large exchange bias after zero-field cooling from an unmagnetized state, *Phys. Rev. Lett.*, 106 (7), 077203.

[51] Suryani, S., Chaerunisaa, A.Y., Joni, I.M., Ruslin, R., Ramadhan, L.O., Wardhana, Y.W., and Sabarwati, S.H., 2022, Production of low molecular weight chitosan using a combination of weak acid and ultrasonication methods, *Polymers*, 14 (16), 3417.

[52] Wang, Y., Li, B., Zhou, Y., and Jia, D., 2009, *In situ* mineralization of magnetite nanoparticles in chitosan hydrogel, *Nanoscale Res. Lett.*, 4 (9), 1041.

[53] Rahmi, R., Fathurrahmi, F., Lelifajri, L., and PurnamaWati, F., 2019, Preparation of magnetic chitosan using local iron sand for mercury removal, *Heliyon*, 5 (5), e01731.

[54] Hao, X., Chen, N., Chen, Y., and Chen, D., 2022, Accelerated degradation of quaternary ammonium functionalized anion exchange membrane in catholyte of vanadium redox flow battery, *Polym. Degrad. Stab.*, 197, 109864.

[55] Grząbka-Zasadzińska, A., Amietszajew, T., and Borysiak, S., 2017, Thermal and mechanical properties of chitosan nanocomposites with cellulose modified in ionic liquids, *J. Therm. Anal. Calorim.*, 130 (1), 143–154.

[56] Sarabandi, K., and Jafari, S.M., 2020, Effect of chitosan coating on the properties of nanoliposomes loaded with flaxseed-peptide fractions: stability during spray-drying, *Food Chem.*, 310, 125951.

[57] Tourrette, A., De Geyter, N., Jocic, D., Morent, R., Warmoeskerken, M.M.C.G., and Leys, C., 2009, Incorporation of poly(*N*-isopropylacrylamide)/ chitosan microgel onto plasma functionalized cotton fibre surface, *Colloids Surf., A*, 352 (1-3), 126–135.

[58] Ardean, C., Davidescu, C.M., Nemeş, N.S., Negrea, A., Ciopec, M., Duteanu, N., Negrea, P., Duda-Seiman, D., and Musta, V., 2021, Factors influencing the antibacterial activity of chitosan and chitosan modified by functionalization, *Int. J. Mol. Sci.*, 22 (14), 7449.

[59] Llanos, J.H.R., de Oliveira Vercik, L.C., and Vercik, A., 2015, Physical properties of chitosan films obtained after neutralization of polycation by slow drip method, *J. Biomater. Nanobiotechnol.*, 6 (4), 276–291.

[60] Tokarčíková, M., Tokarský, J., Kutláková, K.M., and Seidlerová, J., 2017, Testing the stability of magnetic iron oxides/kaolinite nanocomposite under various pH conditions, *J. Solid State Chem.*, 253, 329–335.

[61] Kalska-Szostko, B., Wykowska, U., Piekut, K., and Zambrzycka, E., 2013, Stability of iron (Fe) nanowires, *Colloids Surf., A*, 416, 66–72.